Journal of Physics: Conference Series

PAPER • OPEN ACCESS

Vibration energy flow of main drive system of hot tandem mill

To cite this article: Lidong Wang *et al* 2022 *J. Phys.: Conf. Ser.* **2383** 012160

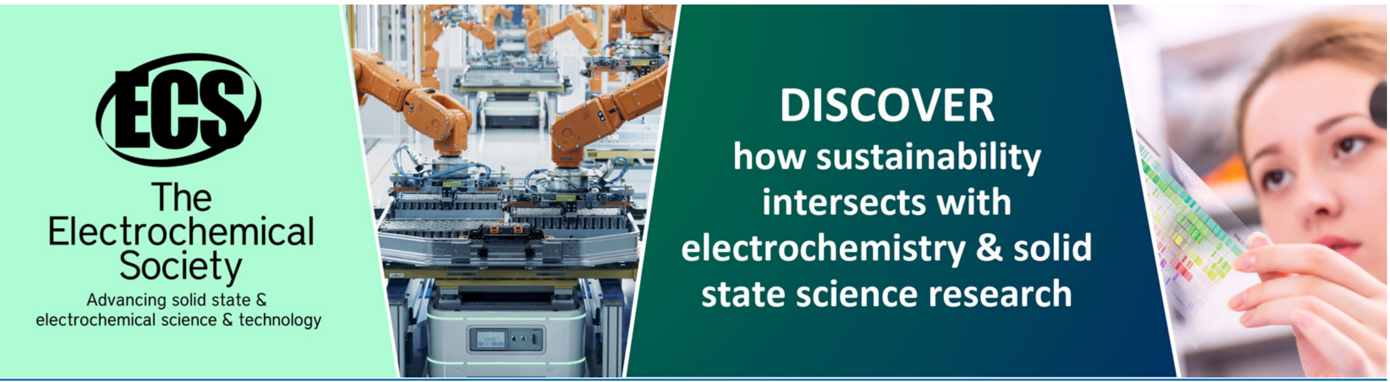

Vibration energy flow of main drive system of hot tandem mill

Lidong Wang[1a*], Xiaoqiang Yan[1b*], Xiaoling Wang[1c]

[1]School of Mechanical Engineering, University of Science and Technology Beijing, Beijing 100083, China

[a*]wld314@163.com, [b*]yxqzhw@126.com, [c]xiaoling@me.ustb.edu.cn

Abstract—We analyzed the power flow of the vibration transmission of the F2 mill drive system coupled with complex beams using the substructure method. The system was divided into three cylindrical substructures, which were coupled to each other by three spring-dampers. The modal analysis of the substructures was conducted to describe their dynamic characteristics; subsequently, the substructure receiving function under free interface conditions was established. The dynamic characteristics of the transmission coupling system were calculated by synthesizing the force balance conditions and geometric coordination at the coupling interface. The input energy and transmission energy in the system were effectively evaluated. The effects of spring-damper stiffness change, excitation position, and loss factor on the transmission of vibration power flow were studied and verified by field experiments. This study provides an effective theoretical basis for vibration suppression measures for hot tandem rolling mills.

1. Introduction

In the thin strip rolling process, ghost vibration of F2 drive system occurs from time to time, and the vibration process is often accompanied by noise. At the same time, the vibration may also transmit the vibration energy to the vertical system through the rolling deformation zone, causing a potential threat of vertical-torsional coupled vibration of the rolling mill. Therefore, it is necessary to reduce the vibration level of the main drive system of the rolling mill.

In the past few decades, the vibration mechanism of rolling mills has been extensively researched. Zhang Ruicheng et al. [1] used the multi-scale method to solve the approximate solution of the electromechanical coupling model of the rolling mill drive system in the case of main parameter resonance. In addition, they employed the numerical method to study the stability of the steady state solution. Yan Peng et al. [2] considered the influence of torque variation under the periodic excitation of the rolling mill drive system and torsional vibration caused by shafting deviation. Zhang Yifang et al. [3] obtained the influence characteristics of different excitation frequency combinations on the rolling mill system by solving the strip-hydraulic reduction excitation model and simulation analysis.

Currently, most of the research work on rolling mill vibration focuses on complex models, such as multi-modal coupling and nonlinear and asymmetric factors [4]. Few studies are based on the coupling effect of energy flow to study the rolling mill vibration. The rolling mill drive is a complex electromechanical structure comprising many substructures, and it is unreasonable to study only the combined characteristics [5]. Therefore, the coupling effect between the motor, gear train, and shaft train should be considered. In particular, it is reasonable to consider the vibration process of the rolling mill as an energy transfer process.

In recent years, vibration power flow has become a powerful tool for analyzing complex nonlinear coupled systems. In this study, the main drive system of the F2 rolling mill, which vibrates most frequently during rolling, is simplified as a coupled beam system. The propagation of vibrational energy in a structure is investigated using a power flow analysis method based on the principle of substructure

2. Model building and response analysis

As shown in Fig. 1, The main drive system of the rolling mill is simply modeled as a cylindrical shell system, because the more detailed modeling of the shafting has slight effect on the analysis results. Therefore, in this analysis, the main drive train of the rolling mill was simplified to three equivalent cylinders, which were connected by two spring dampers, representing the gear train coupling connection between the motor and work rolls. The coupling system is excited at both ends of the drive system to imitate the excitation force of the rolling force of the roll and the torque of the motor. The cylindrical system is shown in Fig. 2. The drive system of the rolling mill can be divided into three subsystems through the substructure-based approach. In this section, through modal analysis, the theoretical receiver function of each substructure system under free interface conditions is established to describe the dynamic behavior.

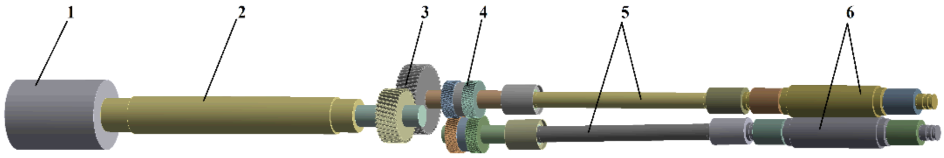

Fig.1 Schematic diagram of F2 drive system
1 – motor; 2 –intermediate handle; 3 – reduction box gear; 4 – herringbone gear seat gear; 5 – universal joint shaft; 6 – work roll

2.1. Substructure method

Since the theory of power flow was proposed in the 1980s, power flow has been widely used in vibration analysis. The transient moment power flow is defined as [5]

$$p(t) = f(t)v(t) \tag{1}$$

However, for the actual structural vibration, the steady-state power flow can effectively describe the actual effect of the vibration, which is defined as the mean value of the vibration energy in a period.

$$P = \frac{1}{2}\mathrm{Re}[F(\omega)v^*(\omega)] = \frac{1}{2}\omega\,\mathrm{Im}[F(\omega)x^*(\omega)] \tag{2}$$

Therefore, the system input power flow is expressed as

$$P_{\mathrm{in}} = \frac{1}{2}\omega\,\mathrm{Im}[F_{in}(\omega)w^*(\omega)] \tag{3}$$

Through path i, the power flow delivered to the end of the path is expressed as

$$P_{trans} = \frac{1}{2}\omega\,\mathrm{Im}[F_{cb}(\omega)u_{cb}^*(\omega)] \tag{4}$$

As shown in Fig. 2, the transmission system of the F2 rolling mill is composed of three sections of simple-uniform supported beams, whose equivalent moments of inertia are I_1, I_2, and I_3, respectively. In the model, the gear pair is considered to be coupled and connected through two sets of spring dampers.

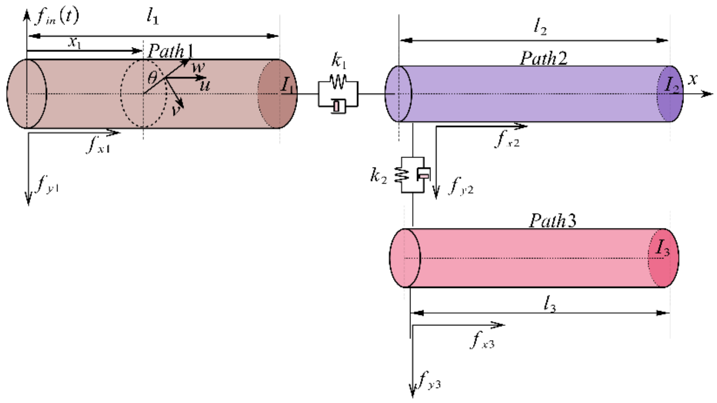

Fig.2 Model of vibration transmission path of F2 rolling mill drive system

The equations of axial and lateral motion of the beam:

$$EI(1+j\eta)\frac{\partial^4 u}{\partial x^4}+\rho A_i\frac{\partial^2 u}{\partial t^2}=f_{in}+\sum_{i=1}^{3} f_{xi}\delta(l_i-x_i) \tag{5}$$

$$EI(1+j\eta)\frac{\partial^4 w}{\partial x^4}+\rho A_i\frac{\partial^2 w}{\partial t^2}=\sum_{i=2}^{3} f_{yi}\delta(l-x_i) \tag{6}$$

where u and w are the axial and lateral displacements of the beam; f_x and f_y represent the axial and transverse excitation forces. l_i is the length of the beam, x_i represents the position of the path, ρ is the density of the beam, E is the modulus of elasticity of the beam, I is the bending moment of inertia, A_i is the cross-sectional area of the beam, η is the loss factor, and δ is the *Delta* function, $j^2=-1$.

Based on the principle of the modal superposition method, displacements u and w are expressed as

$$u(x,t)=\sum_{i=1}^{\infty}\varphi_i(x)p_i(t) \tag{7}$$

$$w(x,t)=\sum_{i=1}^{\infty}\phi_i(x)q_i(t) \tag{8}$$

where $\varphi_i(x)$ and $\phi_i(x)$ are expressed as the beam's axial and transverse mode shape functions, respectively. $p_i(t)$ and $q_i(t)$ are the corresponding modal coordinates.

2.2. Substructure coupling

The three substructures are connected by two pairs of massless spring-dampers. The coupling condition at the spring-damper connection is obtained as

$$F=(W-U)K \tag{9}$$

$$W=[w_1\ w_2\ w_3]\ ;\ U=[u_1\ u_2\ u_3]\ ;F=\begin{bmatrix} f_1\\ f_2\\ f_3\end{bmatrix}\ ;\ K=\begin{bmatrix} k_1(1+j\eta_x)\\ k_2(1+j\eta_y)\end{bmatrix}$$

F is the coupling internal force on transfer path, W ;U is the displacement at the coupling. K is the spring return stiffness. The stiffness of the spring-damper is defined by

$K=K_0(1+i\eta_y)\,\mathrm{N/m^2}$ $K_1=K_2=K_0=4\times10^6\,\mathrm{N/m^2}$

According to [14], the displacement of the beam under the internal coupling force and external excitation has a similar matrix form, as shown below

$$\boldsymbol{U}_{cb}=\boldsymbol{R}_c\boldsymbol{F}_{cb}+\boldsymbol{R}_e\boldsymbol{F}_e,\quad \boldsymbol{U}_{cb}=\begin{bmatrix} u\\ w\end{bmatrix} \tag{10}$$

where $\boldsymbol{R}_{\mathrm{c}}$ and $\boldsymbol{R}_{\mathrm{e}}$ represent the interface receiver functions of coupling force $\boldsymbol{F}_{\mathrm{cb}}$ and the external excitation $\boldsymbol{F}_{\mathrm{e}}$. Eq. (10) expands to

$$\begin{bmatrix} \boldsymbol{U}_{\mathrm{cb}}^{(1)} \\ \boldsymbol{U}_{\mathrm{cb}}^{(2)} \\ \boldsymbol{U}_{\mathrm{cb}}^{(3)} \end{bmatrix} = \begin{bmatrix} \boldsymbol{R}_{\mathrm{c}}^{11} & \boldsymbol{R}_{\mathrm{c}}^{12} & \boldsymbol{R}_{\mathrm{c}}^{13} \\ \boldsymbol{R}_{\mathrm{c}}^{21} & \boldsymbol{R}_{\mathrm{c}}^{22} & \boldsymbol{R}_{\mathrm{c}}^{23} \\ \boldsymbol{R}_{\mathrm{c}}^{31} & \boldsymbol{R}_{\mathrm{c}}^{32} & \boldsymbol{R}_{\mathrm{c}}^{33} \end{bmatrix} \cdot \begin{bmatrix} \boldsymbol{F}_{\mathrm{cb}}^{(1)} \\ \boldsymbol{F}_{\mathrm{cb}}^{(2)} \\ \boldsymbol{F}_{\mathrm{cb}}^{(3)} \end{bmatrix} + \begin{bmatrix} \boldsymbol{R}_{\mathrm{e}}^{1}\boldsymbol{F}_{\mathrm{e}} \\ \boldsymbol{R}_{\mathrm{e}}^{2}\boldsymbol{F}_{\mathrm{e}} \\ \boldsymbol{R}_{\mathrm{e}}^{3}\boldsymbol{F}_{\mathrm{e}} \end{bmatrix} \tag{11}$$

Describing the coupling of three substructures based on force balance and geometric coordination. In spherical coordinates, these conditions for the two spring dampers are expressed as follows

$$\begin{bmatrix} \boldsymbol{T}_{\mathrm{b}}\boldsymbol{F}_{\mathrm{cb}}^{(1)} \\ \boldsymbol{T}_{\mathrm{b}}\boldsymbol{F}_{\mathrm{cb}}^{(2)} \\ \boldsymbol{T}_{\mathrm{b}}\boldsymbol{F}_{\mathrm{cb}}^{(3)} \end{bmatrix} = - \begin{bmatrix} \boldsymbol{K}_1\boldsymbol{T}_{\mathrm{b}}\boldsymbol{U}_{\mathrm{cb}}^{(1)} \\ \boldsymbol{K}_2\boldsymbol{T}_{\mathrm{b}}\boldsymbol{U}_{\mathrm{cb}}^{(2)} \\ \boldsymbol{K}_3\boldsymbol{T}_{\mathrm{b}}\boldsymbol{U}_{\mathrm{cb}}^{(3)} \end{bmatrix} \begin{bmatrix} \boldsymbol{T}_{\mathrm{b}}\boldsymbol{F}_{\mathrm{cb}}^{(1)} \\ \boldsymbol{T}_{\mathrm{b}}\boldsymbol{F}_{\mathrm{cb}}^{(2)} \\ \boldsymbol{T}_{\mathrm{b}}\boldsymbol{F}_{\mathrm{cb}}^{(3)} \end{bmatrix} \tag{12}$$

where T_b is the transformation matrix, Substituting Eqs. (10) and (11) into Eq. (12), the coupling condition becomes

$$\begin{bmatrix} \boldsymbol{T}_{\mathrm{b}}\boldsymbol{F}_{\mathrm{cb}}^{(1)} \\ \boldsymbol{T}_{\mathrm{b}}\boldsymbol{F}_{\mathrm{cb}}^{(2)} \\ \boldsymbol{T}_{\mathrm{b}}\boldsymbol{F}_{\mathrm{cb}}^{(3)} \end{bmatrix} = -[\boldsymbol{K}]\left\{[\boldsymbol{R}_{\mathrm{c}}]\begin{bmatrix} \boldsymbol{T}_{\mathrm{b}}\boldsymbol{F}_{\mathrm{cb}}^{(1)} \\ \boldsymbol{T}_{\mathrm{b}}\boldsymbol{F}_{\mathrm{cb}}^{(2)} \\ \boldsymbol{T}_{\mathrm{b}}\boldsymbol{F}_{\mathrm{cb}}^{(3)} \end{bmatrix} + \begin{bmatrix} \boldsymbol{T}_{\mathrm{b}}\boldsymbol{R}_{\mathrm{e}}^{1}\boldsymbol{F}_{\mathrm{e}} \\ \boldsymbol{T}_{\mathrm{b}}\boldsymbol{R}_{\mathrm{e}}^{2}\boldsymbol{F}_{\mathrm{e}} \\ \boldsymbol{T}_{\mathrm{b}}\boldsymbol{R}_{\mathrm{e}}^{3}\boldsymbol{F}_{\mathrm{e}} \end{bmatrix}\right\} \tag{13}$$

Therefore, the coupled force in spherical coordinates can be written as

$$\begin{bmatrix} \boldsymbol{T}_{\mathrm{b}}\boldsymbol{F}_{\mathrm{cb}}^{(1)} \\ \boldsymbol{T}_{\mathrm{b}}\boldsymbol{F}_{\mathrm{cb}}^{(2)} \\ \boldsymbol{T}_{\mathrm{b}}\boldsymbol{F}_{\mathrm{cb}}^{(3)} \end{bmatrix} = -([\boldsymbol{I}]+[\boldsymbol{K}][\boldsymbol{R}_{\mathrm{c}}])^{-1}[\boldsymbol{K}]\begin{bmatrix} \boldsymbol{T}_{\mathrm{b}}\boldsymbol{R}_{\mathrm{e}}^{1}\boldsymbol{F}_{\mathrm{e}} \\ \boldsymbol{T}_{\mathrm{b}}\boldsymbol{R}_{\mathrm{e}}^{2}\boldsymbol{F}_{\mathrm{e}} \\ \boldsymbol{T}_{\mathrm{b}}\boldsymbol{R}_{\mathrm{e}}^{3}\boldsymbol{F}_{\mathrm{e}} \end{bmatrix} \tag{14}$$

3. Numerical Analysis and Discussion

The input and transmission energy flow of the F2 mill substructure method and the finite element analysis method are first compared through numerical simulation. In addition, the influence of loss factor, excitation position and spring damper stiffness in the driveline model on the vibration power flow transfer is investigated.

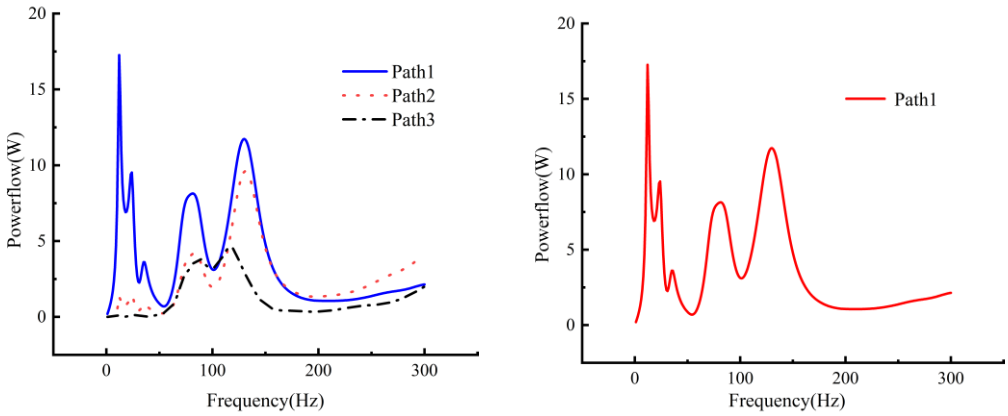

(a) input energy (b) transmitted energy

Fig. 3. Input energy at Path 1 and transmitted energy through three paths

Fig. 3(a) and 4(b) show the time-averaged input energy for Path 1 (motor end) under external excitation, and the variation of the transmitted energy through the motor to the three paths of the upper and lower work rolls. It can be observed that the power transfer through Path 1 is the most dominant.

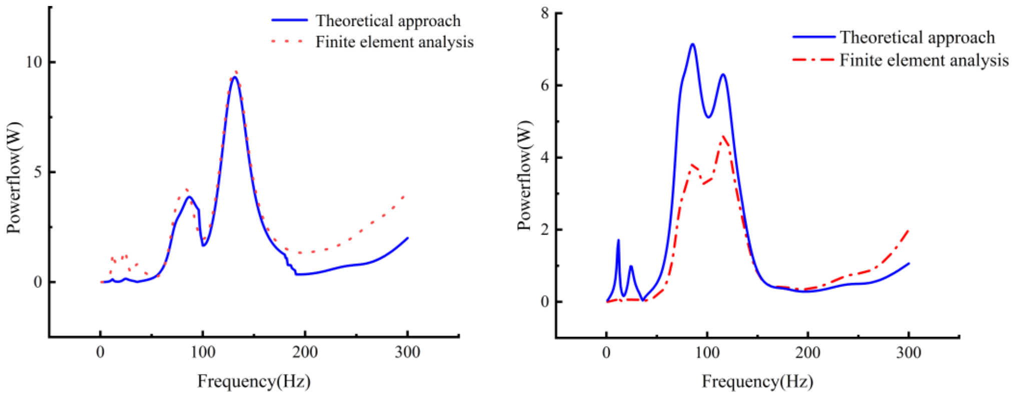

(a) input energy (b) transmitted energy

Fig. 4. Input energy and transmitted energy of Path 2

In Fig. 4, although there is a small amount of error, the input power and transmission power flow of Path 2 calculated by the theoretical methods are typically consistent with the input power and transmission power results of Path 2 through the finite element analysis.

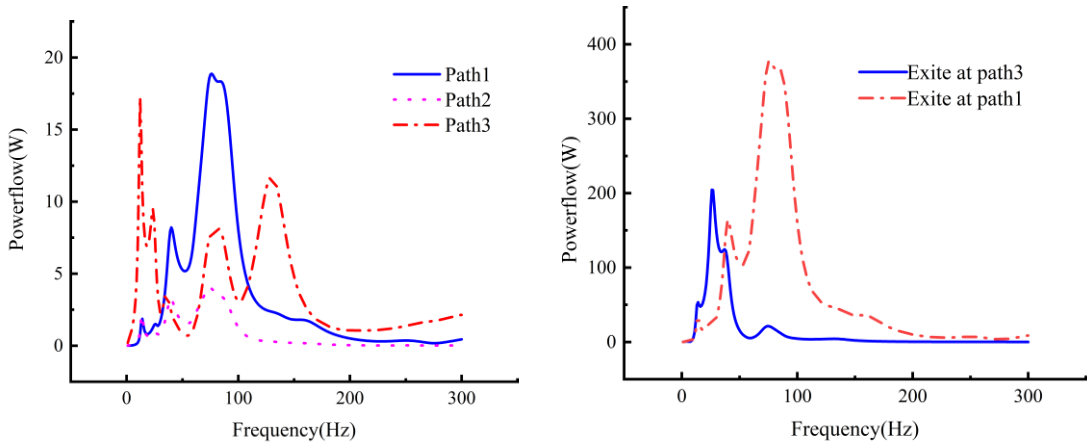

(a) input energy (b) transmitted energy

Fig. 5. Input energy and transmitted energy of Path 3

The transmitted energy through the three paths is shown in Fig. 5(a) during external excitation at Path 3 (the other end of the lower work roll). The transmission energy through Path 3 is dominant at this time. In Fig. 5(b), the input energy is represented during external excitation at Path 1 and Path 3 (work roll end), and it can be observed that Path 1 dominates. Comparing Fig. 3 and Fig. 5, it is found that the path near the excitation position with larger transmission energy dominates. The results in Fig. 5(b) show that the magnitude of the external excitation is the same, but the magnitude of the input energy is different when it is excited at different positions

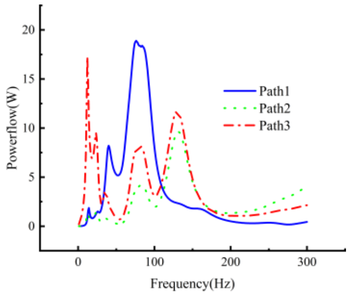

Fig. 6 $K=0.1K_0 \quad \eta=0$

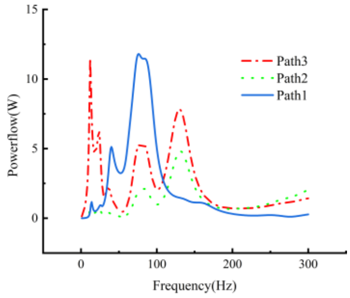

Fig. 7 $K=K_0 \quad \eta=0$

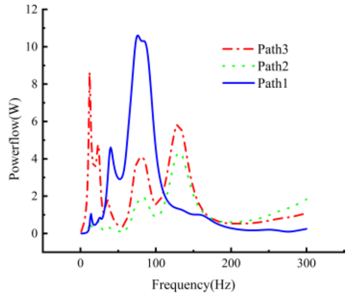

Fig. 8 $K=10K_0 \quad \eta=0$

Using different loss factors and stiffnesses, the effect of spring damper stiffness on the power transfer path is shown. Meanwhile, the external excitation is the simple harmonic excitation force at Path 3. The power flow characteristics under these conditions are shown in Figs. 6, 7, and 8. It can be observed that the position of the energy flow in path 1 can be changed by increasing the coupling stiffness.

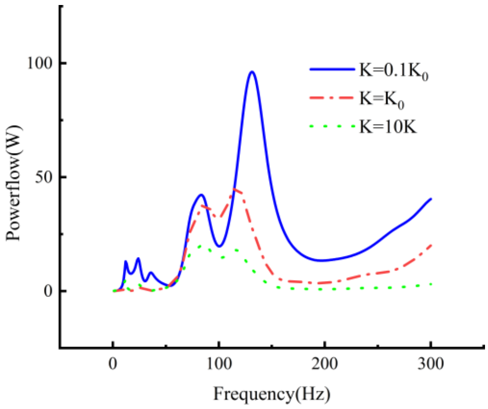

Fig.9 Input energy in three case

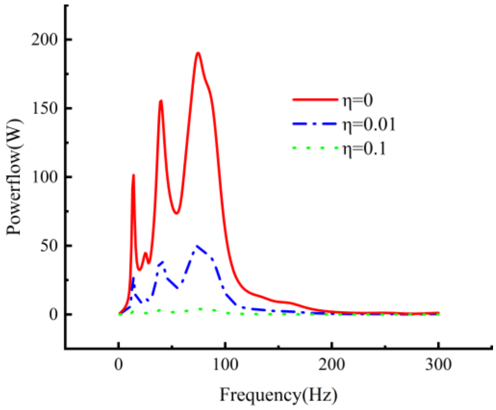

Fig.10 Input energy under different loss factors

From Fig. 9, it can be observed that the spring damper stiffness becomes softer. Therefore, the path input energy flow becomes smaller. In Fig. 10, It can be considered that increasing the damping of the coupled system will greatly reduce the input energy flow. Furthermore, when the damping coefficient is small, the natural frequency of the F2 drive system remains unchanged.

4. Conclusion

In this study, the vibration transmission of the transmission system of the hot tandem mill F2 unit was simplified as a coupled beam system for analysis. Without considering the influence of mill foundation and bearing housing, simplifying the transmission system allows the vibration analysis to be reasonable. Using the substructure method, the vibration power flow transfer is simplified and analyzed. The results showed the input power flow and transmission power in each path. The flow changes all depend on the inherent characteristics of the coupling structure. The vibration transmission is significantly affected by the stiffness and damping of the meshing (equivalent to spring damper) between the gear pairs. Increasing the damping will reduce the input power flow. In addition, the vibration transmission path can be changed by strengthening or softening the meshing state of the gear pair. Although there are certain errors and limitations in this study, the results showed that the analysis of the vibration energy flow characteristics of the rolling mill transmission system based on the substructure simplified system model can provide a theoretical basis for the theoretical analysis of rolling mill vibration and the proposed vibration suppression.

Acknowledgments
This research was funded by the Fundamental Research Fund Project of Central Universities (FRF-AT-19-001).

References

[1] Ruicheng Zhang, Conglin Zhuo. (2016) Parametrically excited vibration of electromechanical coupling system of a rolling mill main drive based on rotor induction current influence. J. Sci. Commun., 35:1-6.
[2] Yan Peng, Jinxing Cui, et al. (2021) Torsional Vibration for Rolling Mill with the Drive System Shaft Axis Deviations. J. Sci. Commun., 46:12165-12177.
[3] Yifang Zhang, Biao Xiao, et al. (2022) Research on vibration of F5 rolling mill in tandem cold rolling under multi-source excitation. J. Sci. Commun., 39:235-243.
[4] Jialei Jiang, Shuang Liu, et al. (2019) Study on vibration characteristics of rolling mill based on vibration absorber. J. Sci. Commun., 5:64-72.
[5] H.G.D. GOYDER, R.G WHITE. (1980) Vibrational power flow from machines into built-up structures, part I: Introduction and approximate analyses of beam and plate-like foundations. J. Sci. Commun., 68:59-75.